Journal of Power Sources 261 (2014) 348–355

Contents lists available at ScienceDirect

Journal of Power Sources

journal homepage: www.elsevier.com/locate/jpowsour

Electrochemical performance of gadolinia-doped ceria (CGO) electrolyte thin films for ITSOFC deposited by spray pyrolysis

Raquel Pereira Reolon [a], Cibele Melo Halmenschlager [a,b,*], Roberto Neagu [b], Célia de Fraga Malfatti [a], Carlos Pérez Bergmann [a]

[a] Department of Materials Engineering, Federal University of Rio Grande do Sul, 9500, Av. Bento Gonçalves – Prédio 74 – Room 211, 91501-970 Porto Alegre, RS, Brazil
[b] National Research Council – Institute for Fuel Cell Innovation, 4250 Wesbrook Mall, V6T 1W5 Vancouver, BC, Canada

HIGHLIGHTS

- Dense and crystalline CGO films deposited by spray pyrolysis on dense and porous substrates.
- Air flow rate has strong influence on the morphology of the film.
- The film has a reasonable electrochemical performance.
- The films obtained are suitable to use as an SOFC electrolyte.

ARTICLE INFO

Article history:
Received 22 October 2013
Received in revised form
20 March 2014
Accepted 22 March 2014
Available online 2 April 2014

Keywords:
Thin films
Gadolinium-doped ceria
Spray pyrolysis
Solid oxide fuel cell
Electrochemical performance

ABSTRACT

Solid Oxide Fuel Cell is an attractive, efficient, alternative source of power generation. However several challenges remained for this technology to be viable. These challenges include high power density, degradation rate, and cost. One way to decrease the SOFC cost is to use stainless steel interconnector. To be able to use a stainless steel interconnector one of the challenges is to find a way to produce an electrolyte, which does not need sintering at high temperature. This work presents the results of the process applied to gadolinia-doped ceria thin films deposited in cycles by spray pyrolysis. The aim of this work was to obtain thin, dense, and continuous CGO coatings, which has electrochemical performance suitable to be used as electrolyte for SOFC. The results obtained show that the air flow rate influenced the droplets size and hence the film quality. X-ray diffraction analysis showed that the films were crystalline after the deposition. Electrochemical tests showed maximum power density of 510 mW cm^{-2} at 650 °C with a thickness average of 3.30 μm when the film was deposited in 12 cycles showing that the film has a potential to be used as an electrolyte for ITSOFC on metal support.

1. Introduction

There is a great interest in research related to alternative forms of electricity production in order to promote increased quantity and quality of energy systems well maintaining and enhancing environmental sustainability [1]. In this context, it is important to develop new technologies for energy generation, especially those from renewable resources [2,3]. Solid oxide fuel cells (SOFCs) are a promising technology for highly efficient power generation from both hydrogen and hydrocarbon fuels, particularly for small units where the efficiency of energy conversion exceeds that of other competing technologies. The operation of SOFCs relies on the ability of certain metal-oxide based ceramics to conduct oxide ions at elevated temperatures. These materials are used as the ion-conducting electrolyte of the fuel cell [4]. Although the performance of high temperature solid oxide fuel cells (SOFCs) at the single cell level has been continuously improved over the past several years problems remain, including high cost, material incompatibility, high ohmic losses and the poor intrinsic fuel utilization due to water vapor produced at the anode [5–7]. Reducing operating temperature of SOFCs down to the range of 500–700 °C will improve long-term performance stability, widen material selection, reduce cost and allow for quicker start-up. It will also decrease electrode sintering, interfacial diffusion between

* Corresponding author. Department of Materials Engineering, Federal University of Rio Grande do Sul, 9500, Av. Bento Gonçalves – Prédio 74 – Room 211, 91501-970 Porto Alegre, RS, Brazil.
E-mail address: cibelemh@yahoo.com.br (C.M. Halmenschlager).

http://dx.doi.org/10.1016/j.jpowsour.2014.03.106
0378-7753/

electrolyte and electrode, and thermal stress in SOFC components, leading to a longer lifetime of the system [8]. To be able to operate an SOFC at lower temperatures (<800 °C) one of the options is the use of thin electrolytes [9]. Thin film materials have microstructural features which are within the nanometer range. To use a thin electrolyte within an SOFC it is necessary that it fills the criteria as follows: operating temperatures of these materials should not undergo drastic changes in their microstructure and coarsening due to Ostwald ripening. The materials and their properties should be stable for at least the expected lifetime of the device [10,11]. The performance of thin membranes, however, is mostly lacking when compared to thick film systems [12]. This can be due to processing related failures such as cracks and pinholes, but also due to the fact that the properties of thin films are often different from bulk material due to strain, degree of crystallinity, porosity, and very small grain size [10].

A solid electrolyte, with higher ionic conductivity than stabilized zirconia, would enable the fuel cell to be operated at lower temperatures for the same thickness of electrolyte [13]. The low internal cell resistance of ceria-based film leads to a higher current density as compared with zirconia based electrolytes. However, the open circuit voltage of ceria-based oxides fuel cell is smaller than the theoretical values, because of partial reduction of the oxide with the fuel [14,15].

Electrolytes made by the classical methods such as tape casting [16] give good power output but has a downside of needing to be sintered at high temperatures making it impossible to use metallic materials as an interconnector [17,18]. A good solution to this problem would be to use a thin film electrolyte that can crystalline at lower temperatures (<900 °C) so it would be possible to keep the ohmic losses to a minimum level and allow the SOFC to operate at lower temperatures reducing the final cost of the device drastically [1,9,19]. Spray pyrolysis has been widely used to produce powders and films because it is an inexpensive and continuous in ambient pressure process [1,20,21]. In this deposition technique, a starting solution containing the precursors is sprayed over a hot substrate by means of a nozzle and assisted by carrier gas. When the fine droplets reach the substrate, the solid compounds react to become a new chemical compound. The quality and the physical properties of the films depend on the deposition parameters such as substrate temperature, molar concentration of the starting solution, post treatment, doped materials, spray rate, type and rate of carrier gas and geometric characteristics of the spray system [22].

This work presents the results of process optimization applied to gadolinia-doped ceria thin films deposited in cycles by spray pyrolysis (SP). The aim of this work was to achieve thin, dense, and continuous CGO coatings, which has an electrochemical performance suitable to use as an electrolyte for SOFC.

2. Experimental

2.1. Spray pyrolysis process

Films obtained in the present work were elaborated from a spray pyrolysis apparatus developed at the National Research Council Canada (NRC-IFCI) and the procedure is described in details elsewhere [23,24]. The precursor solution was deposited on glass slide (J. Melvin Freed Brand, 75 × 25 mm) for parametric study of the deposition parameters. The same solution was deposited on Defect-free, dense, and flat Silicon monocrystal to study the crystallinity after processing, dense alumina (MTI corporation, 0.63 mm thick, 96% purity, surface roughness Ra<1 μm) was used as a substrate for high temperature electrical characterization, and SOFC anode with 57% of NiO and 43% of YSZ [25] were used as anode for electrochemical performance. After each cycle of 2 h each the process was stopped for 10 min to allow the temperature to reach 600 °C, allowing decomposition and crystallization to be completed. This procedure helps to avoid cracks in the CGO layer.

Fig. 1 shows the experimental setup for air blast spray pyrolysis process as well as cell preparation to be test electrochemically.

2.2. Precursor chemistry

The preparation of the precursor solution was previously described [24]. The ammonium cerium nitrate used was from Alfa Aesar, 98%. The gadolinium acetylacetonate with four mol of water was from Strem Chemical, 99.9%. The precursors were dissolved in ethylene glycol mono butyl ether (butyl carbytol, Alfa Aesar, 99%) and ethanol (Fisher Chemical, 90%). Total concentration of the dissolved metal ions was 0.025 mol per liter. Liquid flow rate was kept to 0.04 L per hour and controlled via a syringe pump (SageTM M361). The air flow rate was varied in between 60 L per hour and 105 L per hour. The substrate was heated to 600 °C at rate of 10 °C per minute. The distance between substrate and the nozzle during deposition was 60 mm. A K-type thermocouple was spot welded to the substrate during the deposition process to control the substrate temperature. The temperature of the substrate during the deposition was maintained between 250 °C and 450 °C. The difference in temperature resulted from the scanning of the deposition nozzle.

2.3. Film characterization

Phase and crystalline identification was performed using X-ray diffraction (XRD, Bruker D8 Advance diffractometer) using a Våntec position sensitive detector and a copper cathode with Cu Kα radiation ($\lambda = 0.15418$ nm) with a monochromator with a voltage of 40 kV and a current of 40 mA.

The film morphology and the thickness were investigated by secondary electron microscopy (SEM, Hitachi S-3500N).

One of the most common methods of measuring a thin film resistivity is by using four-point probe method or Van der Pauw method. This method uses probes aligned in a square pattern that contact the surface of the test material. In-plane resistivity was measured between 600 °C and 850 °C (873 K and 1123 K) (by using a van-der-Pauw-type detector with four parallel platinum probes spring loaded to the surface of the deposited film. The van-der-Pauw electrochemical measurement was performed using a Solartron multi-channel potentiostat (Model 1470E). The activation energy (E_a) and the pre-exponential factor (σ_0) in the ionic conductivity region (high oxygen activity) can be obtained by plotting $\ln(\sigma T)$ vs. $1 \times T^{-1}$ [26].

2.3.1. Electrochemical performance procedure

For cell electrochemical measurement the cathode was deposited on the electrolyte by screen printing. More details about the cathode composition may be found in previous work [27]. Cell electrochemical measurement was conducted in a lab-built horizontal button cell test station (Thermcraft incorporated). The cathode was sinterized in situ. The procedure was the following: the cell was heated up to 900 °C at a ramp of 300 °C h^{-1} with 100 ml h^{-1} of oxygen during 2 h. After cathode sintering the cell was cooled down to 650 °C at a ramp rate of 300 °C h^{-1} for a 1 h reduction. The reduction was carried out by anode gas with H_2 concentrations varying per step from 10%, 20%, 40%, 60%, to the final step of 100%, with N_2 balance. Each concentration (balanced by N_2) was held for 15 min. The anode gas was first passed at a flow rate of 100 ml h^{-1} through a bubbler-type humidifier at room temperature. Humidified hydrogen gas (corresponding to 3% H_2O content) was then introduced to the anode side during the cell test. Electrochemical measurements were performed at temperatures of

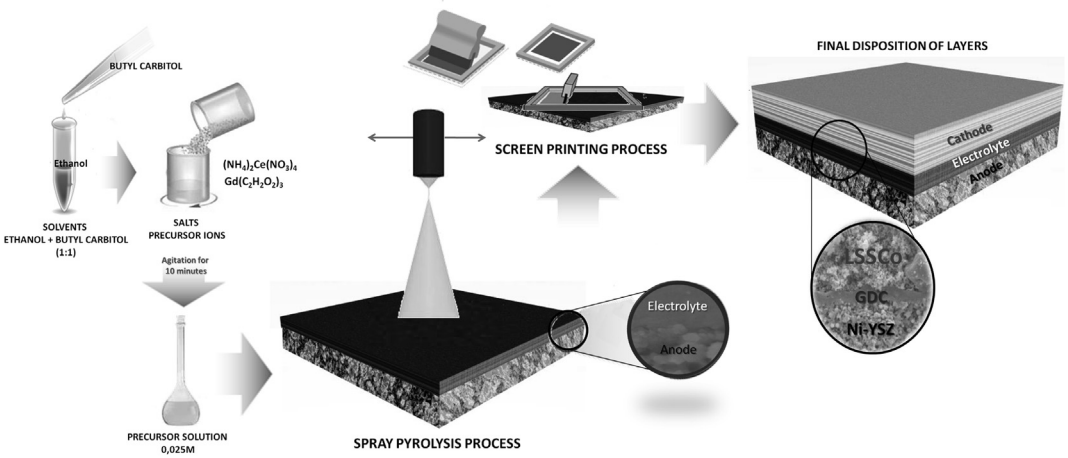

Fig. 1. Experimental setup for spray pyrolysis process and preparation to electrochemical test.

600 °C and 650 °C. *I–V* curve was performed at 600 °C and 650 °C. Cell performance was measured with a Multi-channel Potentiostat/Galvanostat (Solartron 1480 8-channel multi-stat) coupled with a 1260 FRA using the software Corr-Ware and ZPlot. The current–voltage and current–power (*I–V* and *I–P*) curves were obtained using linear sweep voltammetry at a sweep rate of 4 mV s^{-1} from OCV to 0.5 V.

The cell was heated up to 650 °C at a ramp rate of 300 °C h^{-1}, and held at 650 °C for 1 h for reduction and situ sintering of the cathode layer.

The entire experimental procedures and characterization were done at NRC – Institute for Fuel Cell Innovation in Vancouver, Canada.

3. Results and discussion

3.1. Microstructure

Fig. 2 shows the films deposited by spray pyrolysis using different air flow rates. The air flow rate has a reasonable influence on morphology. High air flow rate (Fig. 2b) leads to a quick cooling of the substrate temperature. At the same time droplet size is decreased with high air flow rate. Although coatings deposited with a higher air flow rate (Fig. 2b) has a larger amount of agglomerate than the coatings made with a lower air flow the base layer is crack-free while the base layer of the coating made with a lower air flow rate has some cracks (Fig. 2a). These results may indicate that the droplets formed using 60 L h^{-1} as an air flow rate (Fig. 2a) are too big and that they reach the substrate with a lot of solvent, and may insert cracks into the film layer. In previous work, Muecke et al., have found that the atomization process and the volume deposition are dependent upon the air flow rate and the type of liquid [28]. In further work Muecke et al., found that upon impact droplets spreads on the substrate surface, is heated and the solvent starts to evaporate. When the saturation limit is reached, metal salt or salt decomposition intermediates may precipitate within the droplet and the remaining solvent evaporates, leaving a residue on the surface. The decomposition of the salt or salt intermediate can start at any point during the deposition if the temperature is sufficiently high. Once the deposit is attached to the substrate and is unable to shrink in diameter, the shrinkage associated with salt decomposition causes tensile stresses in the deposits. The stress builds up with every deposited droplet and the film will ultimately crack when the fracture strength of the material is exceeded [29].

According to Perednis and Gauckler, the formation of particles are due to the thermophoretic force pushing the droplets away from a hot surface, because the gas molecules from the hotter side of the droplet rebound with higher kinetic energy than those from the cooler side. The aerosol droplets experience evaporation of the solvent during transport to the substrate. This leads to a size reduction of the droplet and to the development of a concentrated

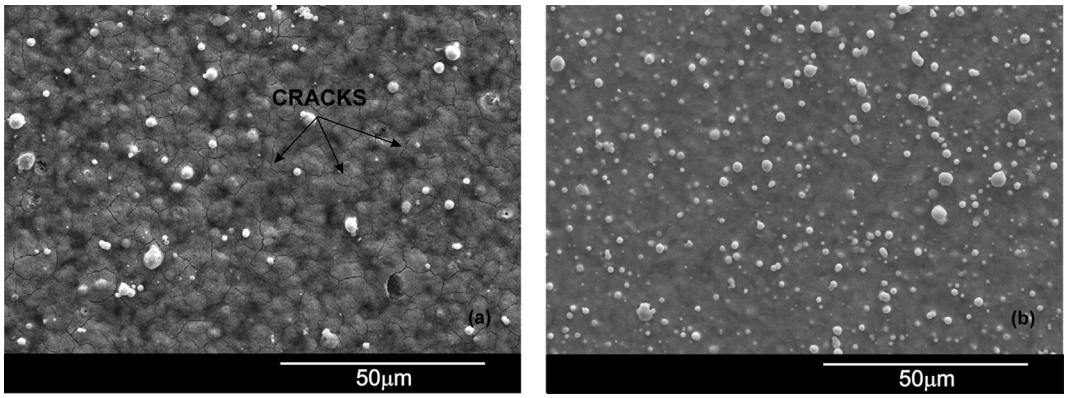

Fig. 2. SEM micrographs of the films deposited on glass slide substrate for a period of 2 h. (a) Using a liquid flow of 0.04 L per hour and air flow of 60 L per hour. (b) Using a liquid flow of 0.04 L per hour and air flow of 105 L per hour.

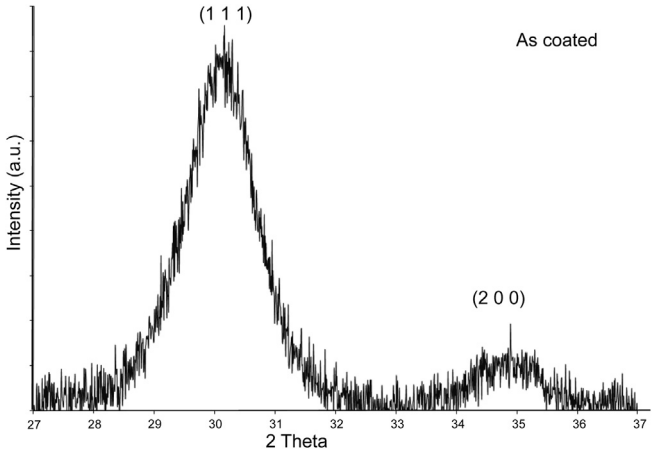

Fig. 3. X-ray diffraction of film as-coated on silicon monocrystal.

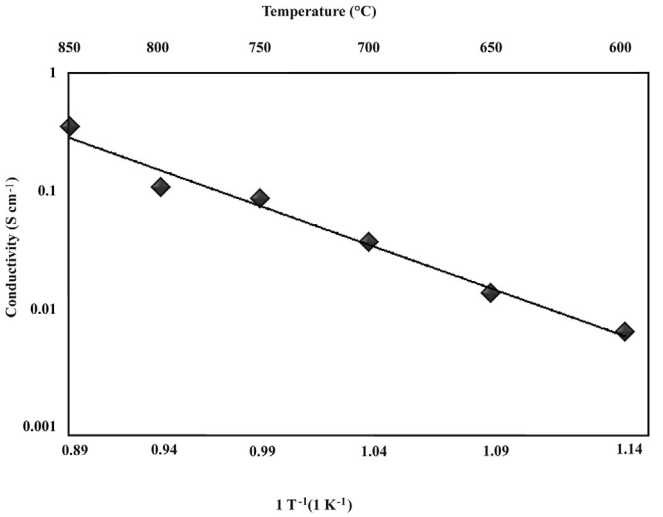

Fig. 5. In-plane conductivity of CGO thin films deposited on alumina substrate as a function of T^{-1}. The film was deposited for a period of 3 h using the liquid flow of 0.04 L per hour and air flow of 105 L per hour.

gradient within the droplet. The precursor precipitates on the surface of the droplet, when the surface concentration exceeds the solubility limit. Precipitation occurs due to rapid solvent evaporation and slow solute diffusion. The results of precursor precipitation within droplets during flight form a porous crust and subsequently hollow particles, which are not desired because they increase film roughness [30]. It is also possible to observe that there are white spots throughout the sample. These white spots are an indication that thickness is uneven. According to previous work uneven thickness is formed when the low boiling point solvent evaporates under boiling while the residue is solidifying, or when salt decomposition time is on the order of the solvent evaporation time [24]. Gaseous reaction products then evolve during solidification, causing a distortion of circular droplet shape. According to Muecke et al., the formation of uneven film surface starts with separate deposits and the surface coverage is less than one monolayer. However, successively arriving droplets selectively deposited on top of the first deposit rather than being deposited randomly, form stacks of deposits on the surface [29].

3.2. Crystallinity

Fig. 3 presents X-ray diffraction pattern of the as-deposited CGO film on silicon monocrystal substrate, where the peak can be assigned to CGO fluorite structure. This result agrees with previous works in the literature [31,32]. The pattern indicates that the film is crystalline after deposition. This result means all decomposition was fully completed and the probability of having cracks in the layers is lower than if the material would have to have a post-heat treatment to crystallize.

3.3. In-plane resistivity

Fig. 4a shows SEM micrographs of the surface and cross-section of CGO thin films deposited on alumina substrates for the van-der-Pauw measurements. It can be seen that the coating is dense, crack-free, and that it contains some aggregated particles. The average film thickness is 1.24 μm (Fig. 4b). It is possible to be seen that the thickness film is not homogeneous. According to Muecke et al., the reason of this uneven coverage is the high temperature. It may disappear if the temperature was lower than what was used in this work. They observed that after the first few minutes of spraying, the substrate surface was randomly occupied with separate deposits and the surface coverage was less than one monolayer. However, successively arriving droplets selectively deposited on top of the first deposits rather than being deposited randomly found that stacks of deposits were formed on the surface [29].

Fig. 5 shows the CGO film conductivity as a function of 1000 T^{-1} in an Arrhenius-type plot. The conductivity of CGO film reaches

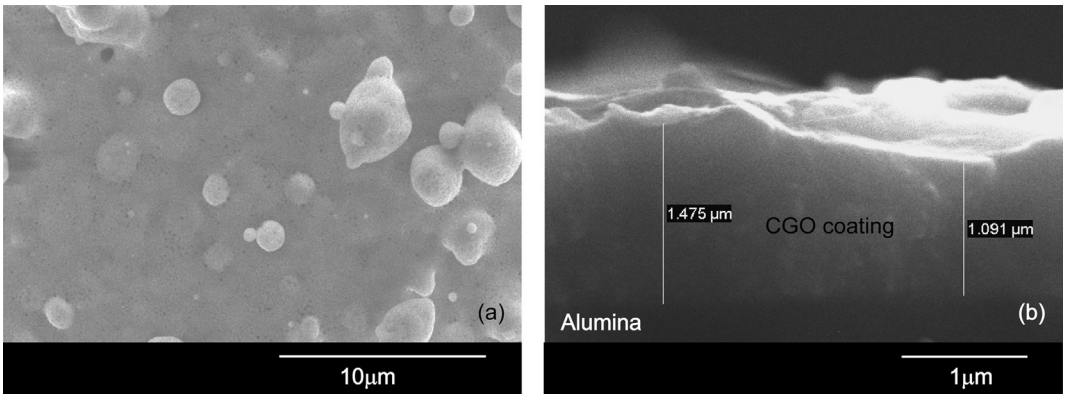

Fig. 4. SEM micrographs of CGO thin films deposited on alumina substrates taken after the van-der-Pauw in-plane resistivity measurement. The film was deposited for a period of 4 h using the liquid flow of 0.04 L per hour and air flow of 105 L per hour. (a) Plan view, (b) cross-section.

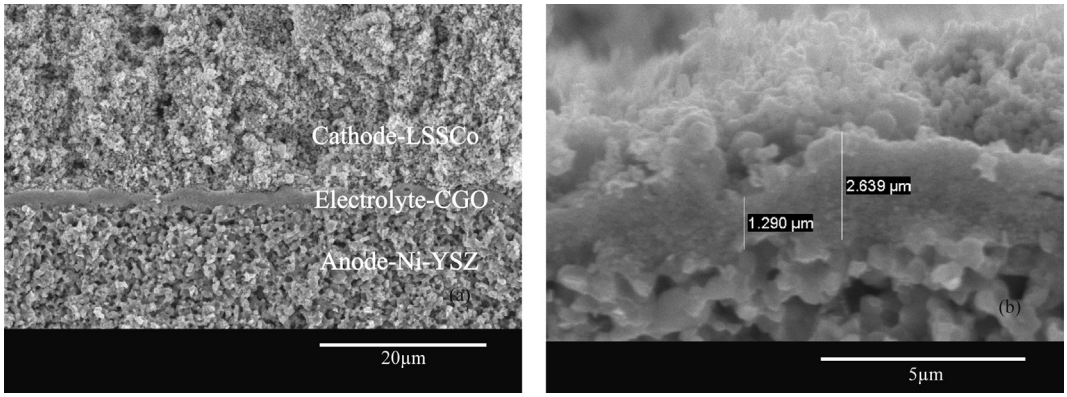

Fig. 6. SEM micrographs cross-section of sample deposited in 5 cycles of 2 h each after being electrochemical tested.

0.11 S cm^{-1} at 800 °C (1023 K) and energy of activation of 126 kJ mol^{-1} at the same temperature. The E_a found in this work is higher than it was expected and possibly it is due to the film may of had a small amount of amorphous phase [12]. This conductivity is better than the conductivity obtained by Zhao and Vikar who could obtain a conductivity of 0.07 S cm^{-1} at 1023 K [33].

3.4. Electrochemical performance

A film to be of use as an SOFC electrolyte and to investigate its performance must be impermeable avoiding contact in between gases which are going to flow at the cathode and anode side [24,34]. As it was shown in a previous work CGO film deposited by a

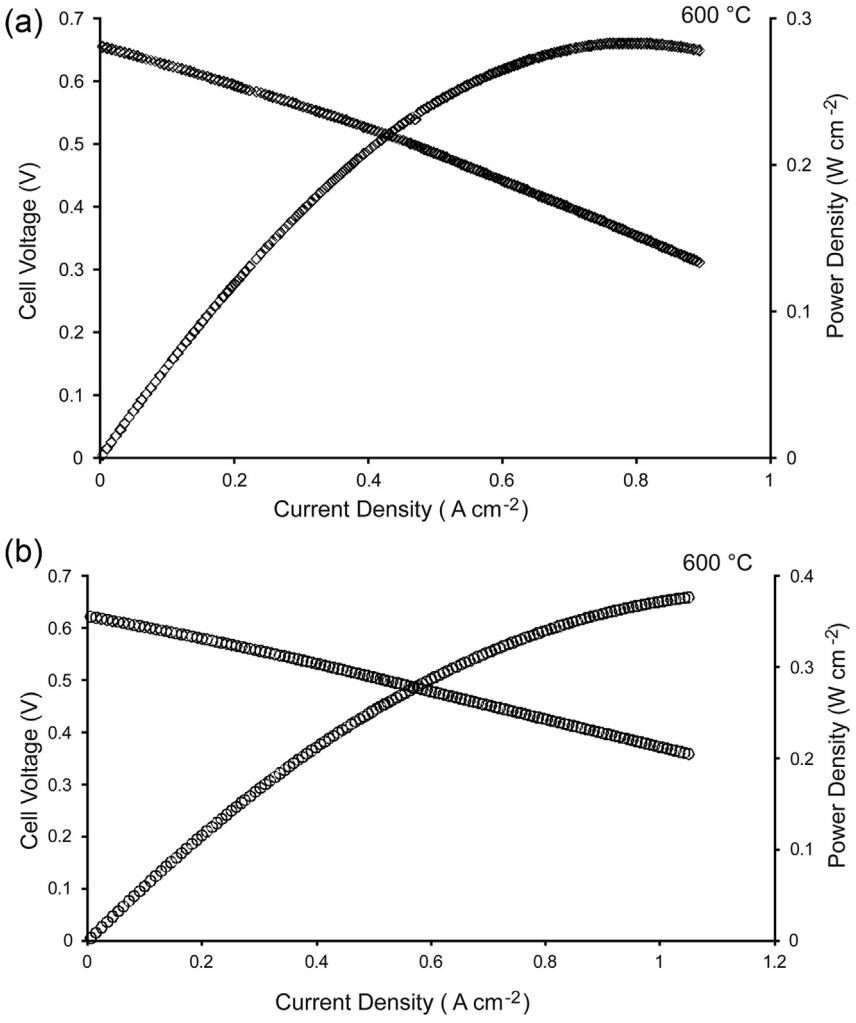

Fig. 7. *I–V* and *I–P* characteristics of anode-supported single cell with the CGO electrolytes deposited in 5 cycles of 2 h each. Test performed (a) at 600 °C and (b) at 650 °C.

continuous spray pyrolysis and thicker than 1.8 μm is impermeable up to 0.01 MPa and it may be used as an ITSOFC electrolyte [24].

Fig. 6 shows the cross-section of the cell after being tested electrochemically. It is possible to see that after 5 cycles the electrolyte is dense and continuous and that it also has an uneven thickness as a film deposited on a dense substrate (Fig. 4b). The average thickness of the electrolyte was 2.08 μm with a standard deviation of 0.488.

The current–voltage–power density characteristics at 600 °C and 650 °C of the anode-supported single cells with the CGO electrolyte film by spray pyrolysis with cathode sintered at 900 °C as shown in Fig. 7a and b, respectively. It is possible to be seen that the cell voltage is 0.67 V at 600 °C and 0.62 V at 650 °C. Usually the low OCV comes from several different factors such as gas leakage due to sealing problems [35]; possible structural defects throughout CGO film, an internal short-circuit due to the partial electronic conductivity [35], permeation of oxygen due to electronic conduction [35], the volume expansion associated with partial reduction of ceria (Ce^{4+} to Ce^{3+}) upon exposure to a reducing atmosphere (e.g., on the anode side exposed to the fuel in an SOFC) may result in severe structural and mechanical degradation (such as micro-crack and delamination) [15]; the change in volume when the anode was reduced from NiO to Ni and its sinterization over time [36]; low electrodes kinetics, interfacial reactions between electrodes/electrolyte, and increasing of electrodes polarization [37]. As shown in previous work electrolytes with an average thickness of 2 μm were gas-tight [24]. This indicates that others factors affects SOFC OCV. Since the electrolyte used in this work was gas-tight the lower OCV probably is coming from an internal short-circuit, fewer defects, interfacial reactions between electrodes/electrolyte, and increasing of electrodes polarization. It is well known that ceria-based electrolytes are mixed ionic-electronic conductors, and that the partial reduction of ceria from Ce^{4+} to Ce^{3+} under reducing conditions gives rise to electronic conduction. The electronic conduction of ceria-based electrolyte results in an internal short-circuit of SOFC, which lowers the OCV of an SOFC [34]. According to Ding et al., CGO electrolytes with a thickness of less than 5 μm show that the cell voltage stays in between 0.7 V and 0.6 V [34].

Duncan et al., also found that for mixed conducting electrolytes (due to the higher mobility of the electronic species), it is possible that the magnitude of the current leakage increases with decreasing thickness faster than the ionic current. Therefore, with mixed conducting electrolytes, the SOFC output power can end up eventually decreasing as the electrolyte thickness decreases [38]. Another source of power losses may be caused by polarizations that are losses in voltage due to imperfections in materials, microstructure, and design of the fuel cell. Polarizations result from ohmic resistance of oxygen ions conducting through the electrolyte, electrochemical activation barriers at the anode [38] and cathode [39], and finally concentration of polarizations due to the inability of gases to diffuse at high rates through the porous anode and cathode [38,39]. OCV is lower than the theoretical value; well maximum power density reached for this sample is reasonable, around 350 mW cm^{-2} at 650 °C (Fig. 7b) and 280 mW cm^{-2} at 600 °C (Fig. 7a) for anode-supported CGO electrolyte single cell.

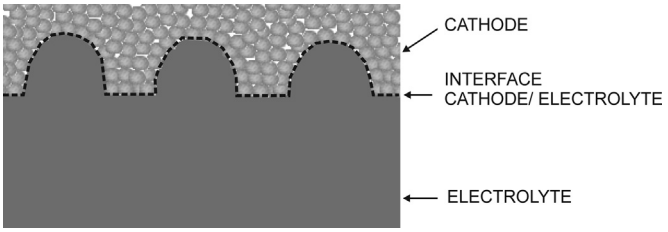

Fig. 9. Schematic drawing of cathode/electrolyte interface.

Fig. 8 shows the cross-section of the cell after being tested electrochemically. In this sample the electrolyte was deposited in 12 cycles of 2 h each. It is possible to see that the electrolyte is dense and continuous. It was expected a thicker film considering that this deposition was made in 12 cycles. However, the average thickness found was 3.25 μm with a standard deviation of 0.759. It is also possible to see that the film is not flat. But this may not be a disadvantage. In a previous work, Ivers-Tiffee et al., show an improvement in an SOFC performance by increasing the number of active reactions sites between cathode and electrolyte [40]. They achieved it by increasing the effective electrolyte surface area and covering the increased surface area with the cathode similar as shown in Fig. 9. As it is possible to see in Fig. 9 represents the morphology achieved at the interface cathode/electrolyte in this work (Figs. 6 and 8). This increasing of active sites may be the cause of having a reasonable performance despite the lower OCV.

Fig. 10a shows that the cell voltage and maximum power density at 600 °C while Fig. 10b shows the cell voltage and maximum power density at 650 °C. Cell voltage is 0.76 V at 600 °C and 0.71 V at 650 °C. It is possible to see that cell voltage is still lower than the theoretical voltage for a single cell using CGO as an electrolyte. The power density has reached 370 mW cm^{-2} at 600 °C (Fig. 10a) and 510 mW cm^{-2} at 650 °C (Fig. 10b). These values are reasonable considering that the cell was not sinterized at high temperatures and the anode can be optimized. The results in this work showed that is very possible to use an electrolyte made by spray pyrolysis in a metal-supported SOFC.

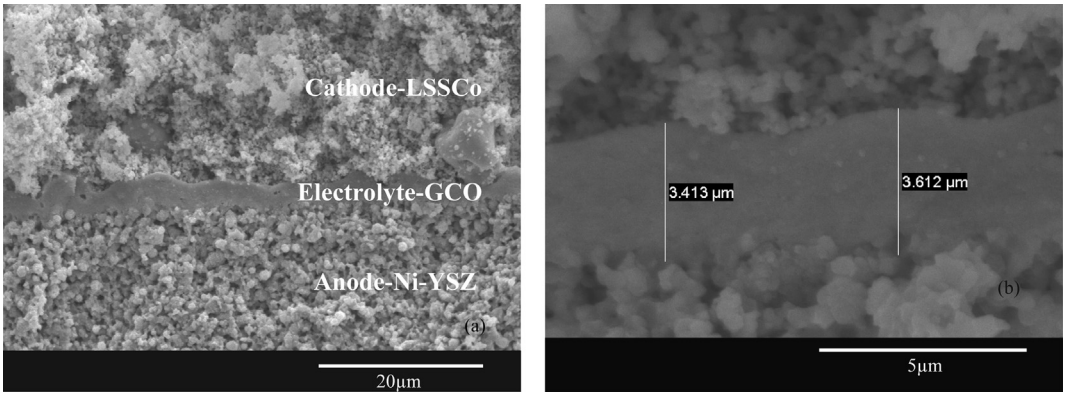

Fig. 8. SEM cross-section of sample deposited in 12 cycles of 2 h each after being electrochemical tested.

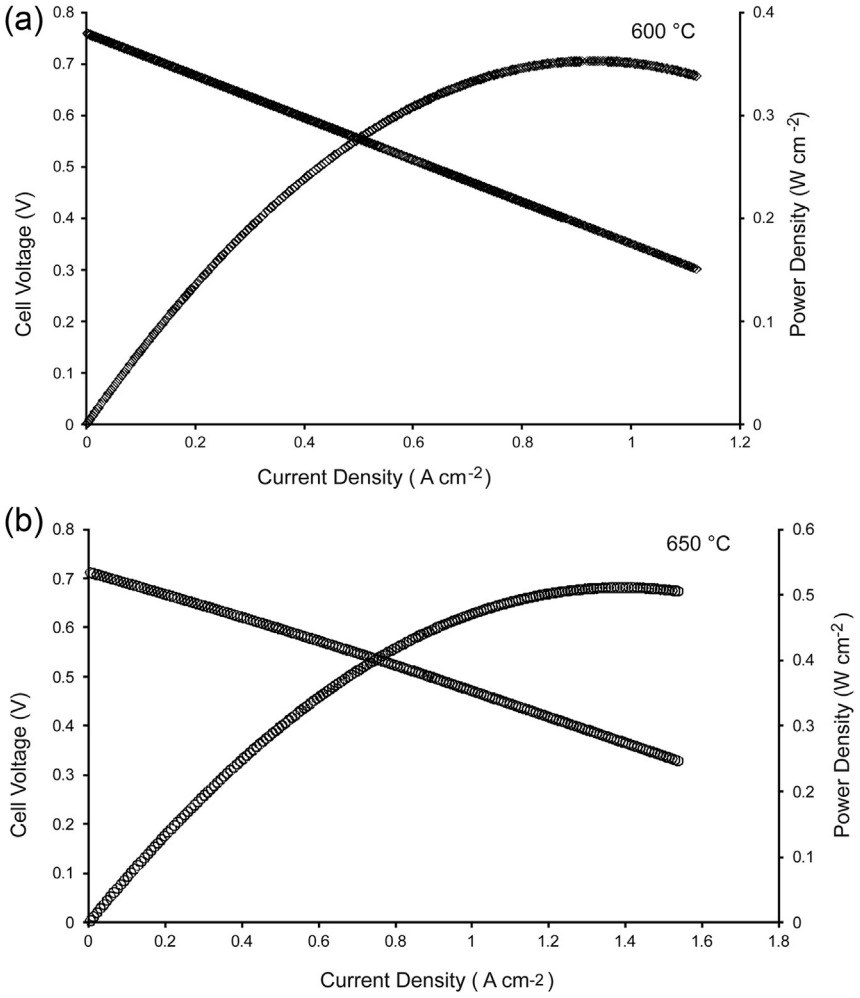

Fig. 10. *I–V* and *I–P* characteristics of anode-supported single cell with the CGO electrolytes deposited in 12 cycles of 2 h each. Test performed at (a) 600 °C and (b) at 650 °C.

4. Conclusions

A spray pyrolysis process in cycles was applied to the preparation of CGO films. The film obtained was dense with or without cracks depending on the air flow rate applied to atomize the precursor solution. XRD analysis showed that the films were crystalline after deposition without requiring post-deposition heat treatment. The conductivity measured by Van der Pauw was 0.11 S cm^{-1} at 800 °C with energy of activation of 126 kJ per mol. The electrolyte thickness had a great influence on cell maximum power density. The maximum power density reached by a single cell using a CGO electrolyte deposited in 5 cycles was 350 mW cm^{-2} at 650 °C and 280 mW cm^{-2} at 600 °C with a thickness average of 2.08 μm. When the film was deposited for 12 cycles the maximum power density reached was 510 mW cm^{-2} at 650 °C and 370 mW cm^{-2} at 600 °C with a thickness average of 3.30 μm. The results show the potential use of the technique of spray pyrolysis to the development of thin films for SOFC.

Acknowledgment

The authors would like to thank engineer Marius Dinus, Jason Fahlman for technical assistance, the Brazilian National Council for Scientific and Technological Development (CNPq) and Coordination for the Improvement of Higher Level -or Education- Personnel (CAPES) for the financial support.

References

[1] D. Perednis, L.J. Gauckler, Solid State Ion. 166 (2004) 229–239.
[2] C.M. Halmenschlager, et al., Nanostructured materials for energy application, nanostructured materials for engineering application, in: M.J. Andrade, C.P. Bergmann (Ed.), Springer-Verlag, Berlin Heidelberg, 2011, pp. 57–73.
[3] G. Bonura, C. Cannilla, F. Frusteri, Appl Catal. B Environ. 121–122 (2012) 135–147.
[4] R.T. Leah, N.P. Brandon, P. Aguiar, J. Power Sources 145 (2005) 336–352.
[5] F. Tietz, V.C.A. Haanappel, A. Mai, J. Mertens, D. Stöver, J. Power Sources 156 (2006) 20–22.
[6] J. Huang, L. Zhang, C. Wang, P. Zhang, Int. J. Hydrogen Energy 37 (2012) 13044–13052.
[7] L. Zhang, W. Yang, Int. J. Hydrogen Energy 37 (2012) 8635–8640.
[8] C. Ding, H. Lin, K. Sato, T. Hashida, J. Membr. Sci. 350 (2010) 1–4.
[9] M.G. Chourashiya, S.H. Pawar, L.D. Jadhav, Appl. Surf. Sci. 254 (2008) 3431–3435.
[10] A. Evans, A. Bieberle-Hütter, J.L.M. Rupp, L.J. Gauckler, J. Power Sources 194 (2009) 119–129.
[11] R. Serra, C. Alves, F.A.C. Oliveira, T. Marcelo, J. Mascarenhas, B. Trindade, Ceram. Int. 38 (2012) 5355–5361.
[12] A. Bieberle-Hütter, P. Reinhard, J.L.M. Rupp, L.J. Gauckler, J. Power Sources 196 (2011) 6070–6078.
[13] A. Moure, A. Castro, I. Martinez, C. Moure, J. Tartaj, Ceram. Int. 38 (2012) 5907–5914.
[14] T. Inoue, T. Setoguchi, K. Eguchi, H. Arai, Solid State Ion. 35 (1989) 285–291.
[15] M. Liu, D. Ding, Y. Bai, T. He, M. Liu, J. Electrochem Soc. 159 (6) (2012) B661–B665.
[16] J.H. Song, S. Park, J.H. Lee, H.S. Kim, J. Mater. Process Technol. 198 (2008) 414–418.
[17] T. Brylewski, M. Nanko, T. Maruyama, K. Przybylski, Solid State Ion. 143 (2001) 131–150.
[18] L. Fan, C. Wang, O. Osamudiamen, R. Raza, M. Singh, B. Zhu, J. Power Sources 217 (2012) 164–169.

[19] B. Huang, X.J. Zhu, Y. Lv, H. Liu, J. Power Sources 209 (2012) 209–219.
[20] C.Y. Chen, T.K. Tseng, S.C. Tsai, C.K. Lin, H.M. Lin, Ceram. Int. 34 (2008) 409–416.
[21] T. Ogi, D. Hidayat, F. Iskandar, A. Purwanto, K. Okuyama, Adv. Powder Technol. 20 (2009) 203–209.
[22] H. Benzarouk, A. Drici, M. Mekhnache, A. Amara, M. Guerioune, J.C. Bernède, H. Bendjffal, Superlattice Microsyt. 52 (2012) 594–604.
[23] Y. Xie, R. Neagu, C.S. Hsu, X. Zhang, C. Decès-Petit, W. Qu, R. Hui, S. Yick, M. Robertson, R. Maric, D. Ghosh, J. Fuel Cell. Sci. Technol. 7 (2010) 021007-1–021007-6.
[24] C.M. Halmenschlager, R. Neagu, L. Rose, C.F. Malfatti, C.P. Bergmann, Mater. Res. Bull. 48 (2013) 207–213.
[25] Xinge Zhang, Mark Robertson, Cyrille Deces-Petit, Yongsong Xie, Rob Hui, Wei Qu, Olivera Kesler, Radenka Maric, Dave Ghosh, J. Power Sources 175 (2008) 800–805.
[26] X.-D. Zhou, B. Scarfino, H.U. Anderson, Solid State Ion. 175 (2004) 19–22.
[27] Xinge Zhang, Mark Robertson, Sing Yick, Cyrille Deces-Petit, Edward Styles, Wei Qu, Yongsong Xie, Rob Hui, Justin Roller, Olivera Kesler, Radenka Maric, Dave Ghosh, J. Power Sources 160 (2006) 1211–1216.
[28] U.P. Muecke, G.L. Messing, L.J. Gauckler, Thin Solid Films 517 (2009) 1515–1521.
[29] U.P. Muecke, N. Luechinger, L. Schlagenhauf, L.J. Gauckler, Thin Solid Films 517 (2009) 1522–1529.
[30] D. Perednis, L.J. Gauckler, J. Electroceram. 14 (2005) 103–111.
[31] I.G. Torregrosa, M.P. Lobera, C. Solis, P. Atienzar, J.M. Serra, Adv. Energ. Mater. 1 (2011) 625–628.
[32] J.L.M. Rupp, A. Infortuna, L.J. Gauckler, Acta Mater. 54 (2006) 1721–1730.
[33] F. Zhao, A.V. Virkar, J. Power Sources 195 (2010) 6268–6279.
[34] C. Ding, H. Lin, K. Sato, K. Amezawa, T. Kawada, J. Mizusaki, Hashida, J. Power Sources 195 (2010) 5487–5492.
[35] J.H. Joo, G.M. Choi, Solid State Ion. 178 (2007) 1602–1607.
[36] M. Mukhopadhyay, J. Mukhopadhyay, A.D. Sharma, R.N. Basu, Solid State Ion. 233 (2013) 20–31.
[37] X. Zhang, M. Robertson, C. Deces-Petit, W. Qu, O. Kesler, R. Maric, D. Ghosh, J. Power Sources 164 (2007) 668–677.
[38] K.L. Duncan, K.-T. Lee, E.D. Wachsman, J. Power Sources 196 (2011) 2445–2451.
[39] M. Odgaard, E. Skou, Solid State Ion. 86–88 (1996) 1217–1222.
[40] E. Ivers-Tiffee, A. Weber, D. Herbstritt, J. Eur. Ceram. Soc. 21 (2001) 1805–1811.